https://doi.org/10.5194/egusphere-2026-4746
Preprint. Discussion started: 28 August 2026

Quantifying 3D topographic effects on geothermal heat flow beneath the Northeast Greenland Ice Stream

Judith Freienstein[1], Charlotte Carter[2,3], Georg Hüttner[1,2], Olaf Eisen[2], Wolfgang Szwillus[1], and Jörg Ebbing[1]

[1]Institute for Geosciences, Kiel University, Kiel, Germany
[2]Alfred Wegener Institute, Bremerhaven, Germany
[3]British Antarctic Survey, Cambridge, England

Correspondence: Judith Freienstein (judith.freienstein@ifg.uni-kiel.de)

Abstract. The North East Greenland Ice Stream (NEGIS) is the largest ice stream in Greenland, and previous studies debate the reasons for its initiation so far into the interior of the ice sheet. Here, we explore how important 3D geothermal heat flow (GHF) is to effective heat transport as a contributing factor. We estimate the effect of high-resolution bed topography on GHF using the finite-element framework pyGIMLi to perform 3D thermal simulations. The bed topography is derived from recent airborne ice-penetrating radar data and covers an area of approximately $40\,x\,60\,\mathrm{km}^2$ surrounding the EastGRIP ice core site at the onset of the ice stream. As large-scale GHF models currently show substantial discrepancies in north-east Greenland, we evaluate the 3D effects for two contrasting background GHF models. Our results show that incorporation of high-resolution bed topography leads to local GHF deviations of up to 20 % relative to background models, closely following topographic patterns. Therefore, incorporating high-resolution GHF, especially in regions with a large ice flux, could reduce uncertainties in our understanding of the origin and stability of ice streams. However, for the NEGIS itself, our preferred background model of low GHF implies that topographic effects channeling GHF do not significantly alter the behavior of the ice stream.

1 Introduction

The Greenland Ice Sheet (GrIS) is a major contributor to global mean sea level rise through ice mass loss (Otosaka et al., 2022), where ice streams account for around 50% of this mass loss through dynamic discharge (IMBIE Team, 2020). An example is the Northeast Greenland Ice Stream (NEGIS), an approximately 600 km long fast flowing ice stream that constitutes a major drainage system of the GrIS (Krieger et al., 2020) (Fig. 1). The geometry of the NEGIS differs from other topographically unconstrained glaciers in Greenland because it exhibits clearly defined shear margins. Other streams are typically wider and exhibit convergent flow into a main trunk (Chu et al., 2018). Thus, its origin remains enigmatic and has been a long-standing subject of discussion (Zhang et al., 2025; Franke et al., 2021; Holschuh et al., 2019).

A still debated explanation for the origin of this fast flowing ice stream so far into the interior of the GrIS is elevated geothermal

https://doi.org/10.5194/egusphere-2026-4746
Preprint. Discussion started: 28 August 2026

heat flow (GHF) beneath its onset region (Fahnestock et al., 2001; Rysgaard et al., 2018). As a thermal boundary condition at the ice-bedrock interface, GHF plays an important role in describing the basal state of the ice (Colgan et al., 2022; Reading et al., 2022). For the NEGIS in particular, previous studies have shown that the choice of the GHF model significantly influences the hydrological system (Smith-Johnsen et al., 2020b).

However, the magnitude of GHF required to sustain the NEGIS remains highly uncertain and is debated. Smith-Johnsen et al. (2020a) couple ice sheet dynamics with a subglacial hydrology system and suggested that an extremely high local GHF (970 $\mathrm{mW\,m^{-2}}$) at the base is required to reproduce the observed ice flow velocities at the NEGIS. Such values have been questioned as geologically improbable (Bons et al., 2021). Other studies propose elevated, but more moderate and geologically more realistic, GHF values on the order of 130 $\mathrm{mW\,m^{-2}}$ for northeast Greenland (e.g. Greve, 2019).

Only a few observations are available to constrain the heat flow beneath the GrIS, making especially spatial interpolations between observations highly uncertain. Individual observations with high uncertainties can therefore strongly influence regional GHF estimates. A prominent example is the observation at the NorthGRIP ice core site. Its value significantly exceeds the Greenland mean of approximately 60 $\mathrm{mW\,m^{-2}}$ (Colgan et al., 2022) and lies outside the typical ranges expected for the continental crust based on the statistics of the thermal parameters (Freienstein et al., 2024). From a geophysical and geostatistical perspective, such elevated values can represent a local anomaly or measurement uncertainty and therefore require careful consideration when used in regional GHF models (Colgan et al., 2022; Freienstein et al., 2024). Consistent with this interpretation, lithospheric modeling studies (Wansing et al., 2024; Martos et al., 2018; Ajourlou et al., 2025) do not unequivocally support the presence of a geothermal hot spot beneath northeast Greenland, and the most recent models argue against this. Consequently, a recent moderate large-scale GHF model that excludes this observation does not show an indication of unusually high GHF in the NEGIS region (Colgan et al., 2022), suggesting that elevated regional geothermal heat flow is unlikely to be the main driver of the NEGIS. In addition, present models are limited in their spatial resolution and provide large scale constraints ($>$55 km), rather than local scales ($<$10 km) required to resolve processes beneath ice streams. However, small-scale variability in GHF may strongly influence the origin, flow pattern, or velocity of ice streams (Aschwanden et al., 2016). McCormack et al. (2022) demonstrated that neglecting small-scale variations of GHF can lead to an underestimation of basal melt rates and suggest that GHF variations on a spatial scale of 20 km or less should be considered. This variability may arise from geological and morphological heterogeneity (e.g. Slagstad et al., 2009), including variations in radiogenic heat production (e.g. Lösing et al., 2025a; Li and Aitken, 2024), the presence of sediments (e.g. Wangen, 1994), or variations in bed elevation (e.g. Colgan et al., 2021). In particular, bed elevation can introduce systematic 3D conductive effects that modify the spatial distribution of GHF on a kilometer scale. Unlike many poorly constrained subsurface parameters, high-resolution bed elevation is increasingly available for Greenland, making bed topography a suitable parameter for investigating small-scale variability in 3D models of GHF.

In this study, we used three-dimensional thermal forward modeling for the NEGIS onset region. Recently published high-resolution subglacial bed topography derived from swath radar surveys (Carter et al., 2025b) provides an opportunity to directly investigate the influence of bedrock topography on GHF at kilometer-scale resolution. To account for the contrasting large-scale GHF models, we evaluate the 3D effects on GHF with two large-scale heat flow models as background: (1) the

https://doi.org/10.5194/egusphere-2026-4746
Preprint. Discussion started: 28 August 2026

moderate GHF model of Colgan et al. (2021), which does not indicate elevated GHF beneath the NEGIS and (2) the GHF model of Greve (2019), which predicts comparatively higher GHF at the NEGIS. The resulting high-resolution GHF models are compared with the topographic correction proposed by Colgan et al. (2021) to empirically estimate the topographic influences on geothermal heat flow. Finally, we calculate the resulting basal melt rates following the approach of Karlsson et al. (2021). This analysis provides new insights into the 3D effects of bed elevation on GHF and the potential influence on basal melting and ice dynamics in the NEGIS region. It highlights the advantage of fully resolved 3D calculations for local studies compared to empirical correction approaches.

2 Data and Methods

In this section, we describe the datasets and modeling approach used to estimate GHF in the onset region of the NEGIS. The study area is centered on the EastGRIP ice core site (Fig. 1), where high-resolution bed topography data allow for 1D and 3D thermal modeling.

2.1 Methods

The pyGIMLi package (Rücker et al., 2017) uses finite elements to solve for the temperature distribution in a 3D space. The model set-up with the 3D volume is shown in Fig. 2(a).

The model domain is discretized using an unstructured tetrahedral mesh with increased resolution in the vicinity of interfaces to accurately resolve temperature gradients. We use a lateral resolution of 1 km for bed elevation, 5 km at the Moho depth and 10 km at the LAB (lithosphere-asthenosphere boundary), as the base of the model. The individual layers are isotropic. To avoid edge effects, we extend the model outside the desired region to get a box with 100 km x 100 km x 300 km. We apply Dirichlet boundary conditions with $0°$C, representing the pressure melting point, at the bed topography and $1315°$C at the LAB depth and insulate the model at the top, bottom, and sides by setting the thermal conductivity $k_{insulate} = 0.1\,\mathrm{W\,m^{-1}K^{-1}}$. This setup ensures that lateral heat flow across the model boundaries is negligible within the target region.

The thermal conductivities for the crust and the mantle are constant with $k_1 = 2.7\,\mathrm{W\,m^{-1}K^{-1}}$ and $k_2 = 3.0\,\mathrm{W\,m^{-1}K^{-1}}$. Radiogenic heat production (RHP) is assumed to be laterally variable but constant in depth and limited to the layer between the bed topography and the Moho boundary. We calculate the RHP from large-scale GHF models to account for the background GHF (Fig. 3(a), (c)). Here, we do not include the bed topography, as the RHP should only account for the large-scale trend of the GHF. This parameterization follows the commonly adopted assumption of depth-averaged crustal heat production (e.g. Lachenbruch, 1970), and allows for direct comparison with reduced one-dimensional formulations. The resulting 3D GHF is computed from the vertical component of the temperature gradient evaluated at points located slightly below the model surface (5 m) to avoid numerical artifacts associated with boundary interpolation.

For comparison, we calculate the GHF with the 1D steady state stationary heat equation, adapted from Lachenbruch (1970) as used in Freienstein et al. (2025):

https://doi.org/10.5194/egusphere-2026-4746
Preprint. Discussion started: 28 August 2026

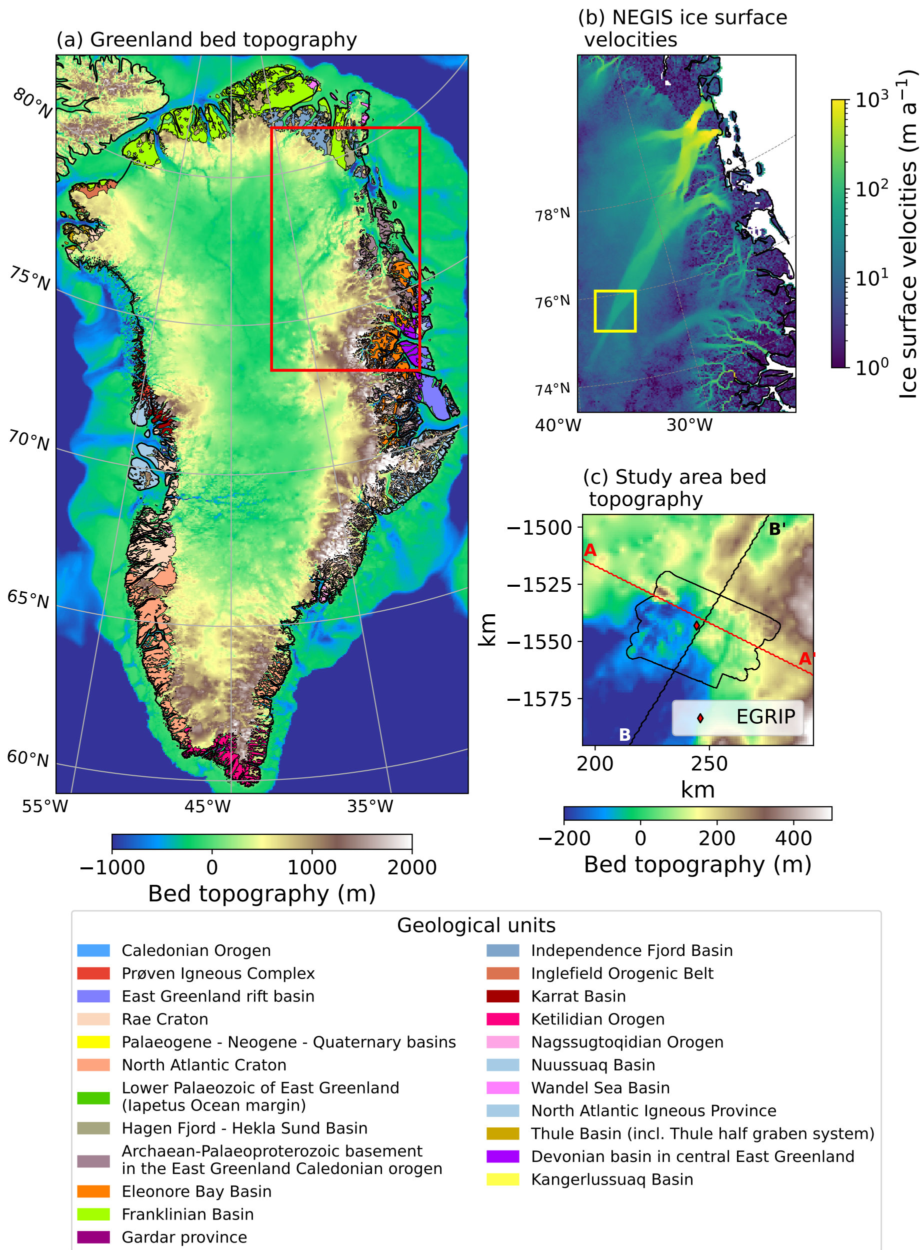

Figure 1. Overview of the study area. (a) BedMachine v5 bed elevation of Greenland (Morlighem and et al., 2022) together with the known geology (Henriksen et al., 2009). The red rectangle indicates the location of the NEGIS overview shown in panel b. (b) Ice surface velocities (Gardner et al., 2024) of the NEGIS. The yellow rectangle marks the extent of the study area displayed in panel c. (c) Bed elevations of the study area including the outline of the high-resolution model domain. The red and black lines indicate profiles A-A' and B-B', respectively, which are used for the later two-dimensional presentation of model results.

https://doi.org/10.5194/egusphere-2026-4746
Preprint. Discussion started: 28 August 2026

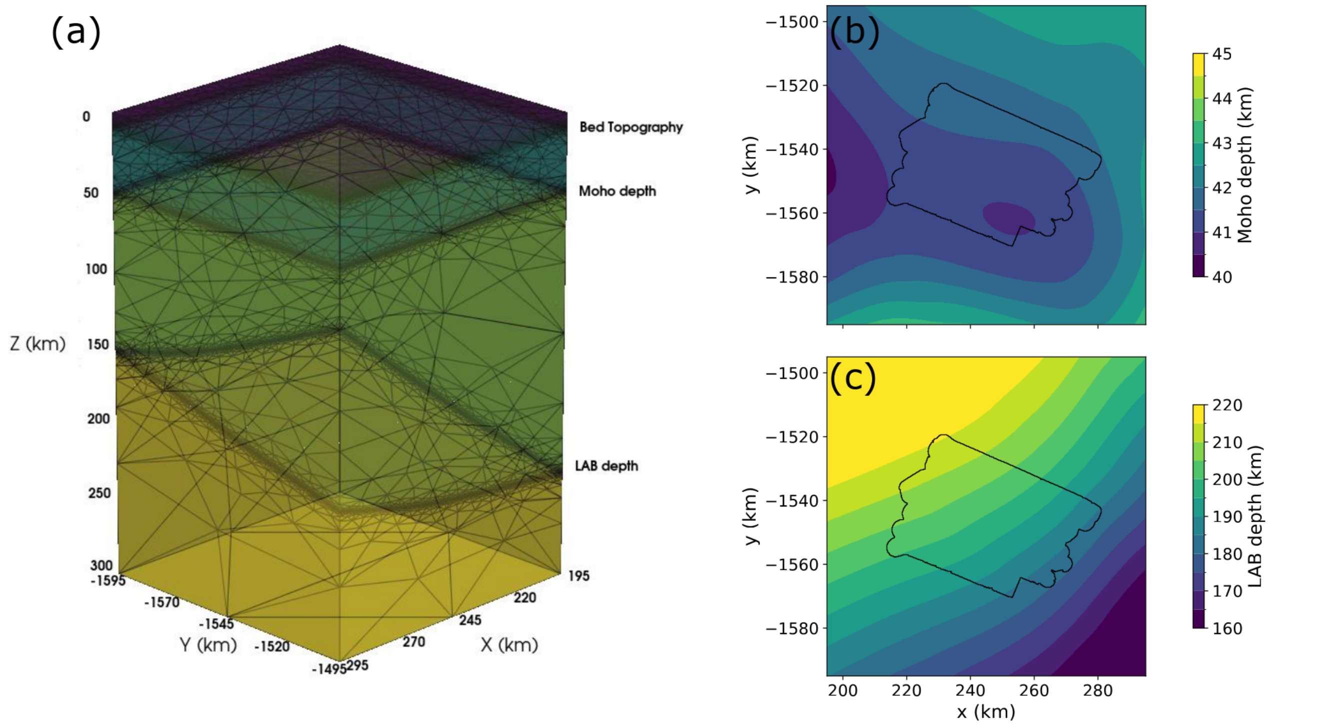

Figure 2. (a) Three-dimensional finite-element mesh grid used for the thermal modeling of the NEGIS region. The model domain covers the study area and is discretized using unstructured tetrahedral elements. Lithospheric layers are included in the model and the vertical subdivision and mesh refinement are illustrated. (b) shows the Moho depth and (c) the LAB depth of the study area.

$$q_{0,1D} = -\frac{(T_{\text{LAB}} - T_{\text{surface}}) + \dfrac{A\,D_c\,D_m}{k_2} + \dfrac{1}{2}\,\dfrac{A\,D_c^2}{k_1}}{\dfrac{D_m}{k_2} + \dfrac{D_c}{k_1}} \tag{1}$$

with

$$D_c = z_{\text{Moho}} - z_{\text{surface}}, \qquad D_m = z_{\text{LAB}} - z_{\text{Moho}}$$

with temperatures T_i, depths z_i, thicknesses of the crust and mantle D_c and D_m, thermal conductivities k_i and radiogenic heat production A.

This 1D model is stationary and includes purely vertical heat transport and no advection. We use the same parameters as for the 3D model.

https://doi.org/10.5194/egusphere-2026-4746
Preprint. Discussion started: 28 August 2026

2.2 Data

The high-resolution subglacial topography was observed using the Alfred Wegener Institute's ultra-wideband radar system (AWI-UWB), using swath radar processing techniques to map the cross-track bed elevation at a swath width of 2 km (Carter et al., 2025b, a). This produces a $40\,x\,60\,\mathrm{km}^2$ Digital Elevation Model (DEM) with a horizontal resolution of 25 m and a vertical uncertainty of 10 m. For our purpose, we apply a Gaussian low-pass filter with a cut-off wavelength of 3000 m to suppress small anomalies and artifacts of the swath processing and resample the data at a lateral resolution of 200 m. Additionally, we extend the high-resolution subglacial topography by merging it with the bed topography of BedMachine v5 (Morlighem et al., 2017) to minimize edge effects within the 3D calculations (Fig. 1(c)). The BedMachine bed topography has poor data coverage especially in our study area but still sufficiently reflects the larger trend of the bed elevation. We correct for an observed shift of approximately 30 m between both data sets that results from the use of the geoid as the reference height in BedMachine v5 and the ellipsoid as the reference height in the swath radar-generated DEM.

Information on Moho and LAB depths (Fig. 2(a) and (b)), as well as the thermal conductivities for the crust and mantle, are taken from the lithospheric scale model of Wansing et al. (2024).

We use two different large-scale GHF models as a basis for our calculations. Colgan et al. (2022) use a machine learning approach that incorporates in situ GHF observations and other geophysical datasets, such as Moho and LAB depth, seismic, magnetic, and gravity data, and the distance to major tectonic features to derive the GHF. We use the GHF model of Colgan et al. (2022) without NGRIP as the observed high ice borehole measurement at NGRIP, as this observation is highly uncertain and should be excluded from regional GHF models (Colgan et al., 2022; Freienstein et al., 2024). The cold GHF model shows a mean GHF of approximately $40\,\mathrm{mW\,m^{-2}}$ in our study area (Fig. 3(a)). The contrasting model of Greve (2019) with the higher large-scale GHF (Fig. 3(c)) is derived using a spherical-harmonic background model and paleo-climate ice sheet simulations to fit the simulated and observed basal temperatures by modifying the GHF at five deep ice core locations. This warm GHF model has a mean GHF of approximately $100\,\mathrm{mW\,m^{-2}}$ in our study area.

3 Results

3D and 1D comparison

We calculate the 3D and 1D GHF for the two background GHF models. We compare the 1D and 3D results for a cold GHF model and for a warm GHF model (Fig. 4). Both cold 1D and 3D approaches yield a mean GHF of approximately $40\,\mathrm{mW\,m^{-2}}$. The mean GHF for both the warm 1D and 3D models is approximately $98\,\mathrm{mW\,m^{-2}}$.

Recalculating the GHF with high-resolution bed elevation included in the 1D steady-state heat equation does not alter the GHF, closely reflecting the respective background model. In the 3D model, the influence of the bed topography is reflected in deviations of approximately $\pm 10\,\mathrm{mW\,m^{-2}}$ for the cold model and $\pm 20\,\mathrm{mW\,m^{-2}}$ for the warm model, which are more pronounced in the area with high resolution topographic data. By comparing our GHF models derived from high-resolution

https://doi.org/10.5194/egusphere-2026-4746
Preprint. Discussion started: 28 August 2026

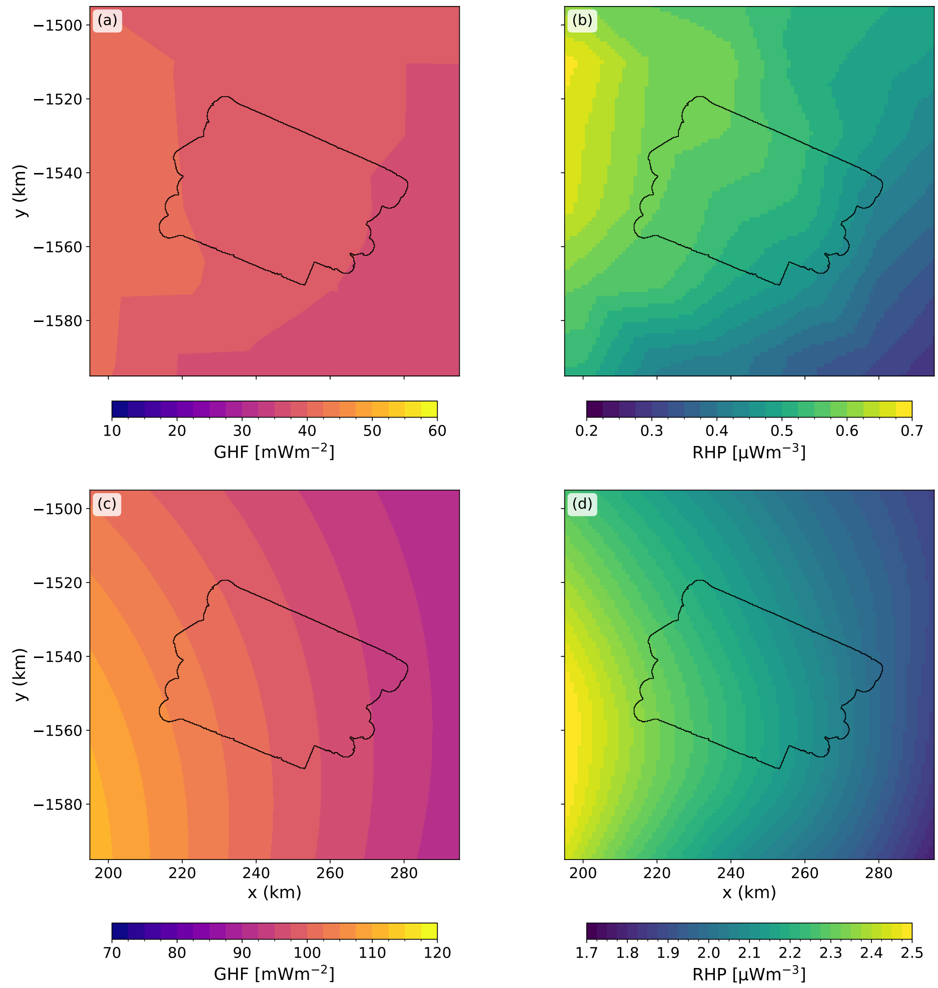

Figure 3. (a) the GHF from Colgan et al. (2022) for the study area. (b) The calculated RHP for the cold model. (c) the GHF from Greve (2019) for the study area. (d) The calculated RHP for the warm model. The outline of the high-resolution model domain in highlighted.

bed topography with corresponding models based on the lower-resolution BedMachine dataset (Appendix B), we show that higher topographic resolution substantially increases the spatial detail of the GHF field, resulting in differences exceeding 10 % amplitude of the overall GHF at small spatial scales. Comparing the cold and warm 3D models, both show similar small-scale patterns (Fig. 5 (a), (b)). However, the warm model exhibits significantly larger deviations(Fig. 5 (b), (c)). This increase can be explained by the generally higher background GHF. Both models show a clear anti-correlation between the bed topography and GHF (Fig. 5 (d), (e)). The relative contributions of the 3D effects to the respective 1D models are comparable in magnitude and spatial pattern (see Appendix A). The difference map (Fig. 5(c)) reveals variations at large-scales between the two models that cannot solely be explained by the geometric effect of topography in 3D calculations. 2D profiles (profiles A and B in Fig. 1(c)) across (Fig. 6(a)-(d)) and along (Fig. 6(e)-(h)) the direction of the ice stream highlight the effect of bed elevation

https://doi.org/10.5194/egusphere-2026-4746
Preprint. Discussion started: 28 August 2026

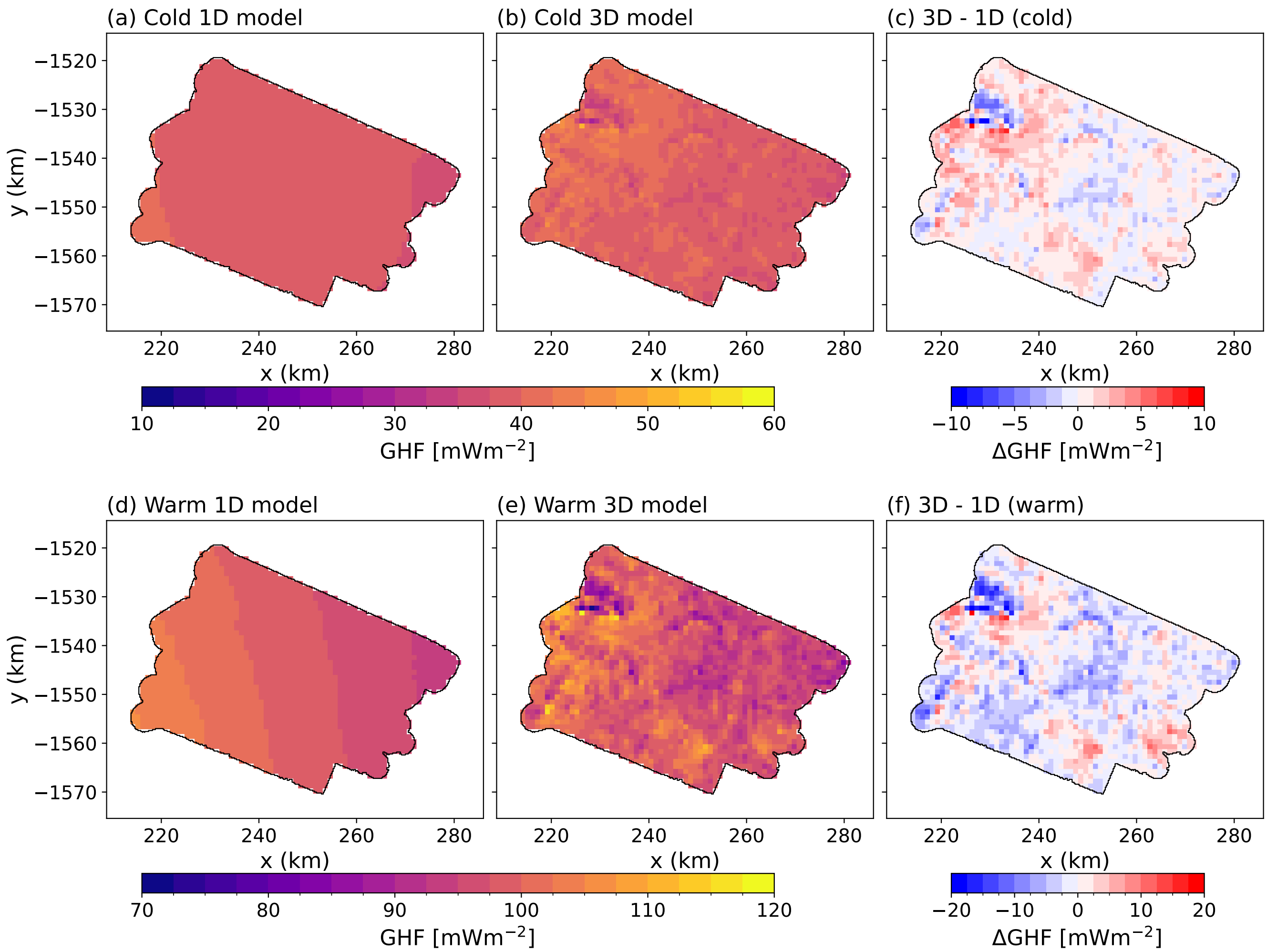

Figure 4. Comparison of (a) the calculated 1D and (b) 3D cold GHF model. Both models include the bed elevation. The difference between the calculated 1D and 3D model is shown in (c). (d) - (f) show the respective results for the warm GHF model.

on 3D GHF. In particular, regions with abrupt topographic changes (e.g., Fig. 6, profile B, profile distance 35-40 km) show pronounced influences of bed elevation on small-scale GHF. These effects are stronger for warmer background GHF models.

The amplitudes of the peaks increase significantly with higher background GHF, while their spatial distribution remains consistent. The large-scale GHF pattern mainly follows the large-scale trend of the bed elevation and a decrease in 1D GHF, and thus RHP with larger profile distances. The temperature profiles (Fig. 5(c), (d), (f), (g))) demonstrate that the topographic pattern is visible in greater depths and highlight the effect of the different background GHF on the general temperature gradients.

https://doi.org/10.5194/egusphere-2026-4746
Preprint. Discussion started: 28 August 2026

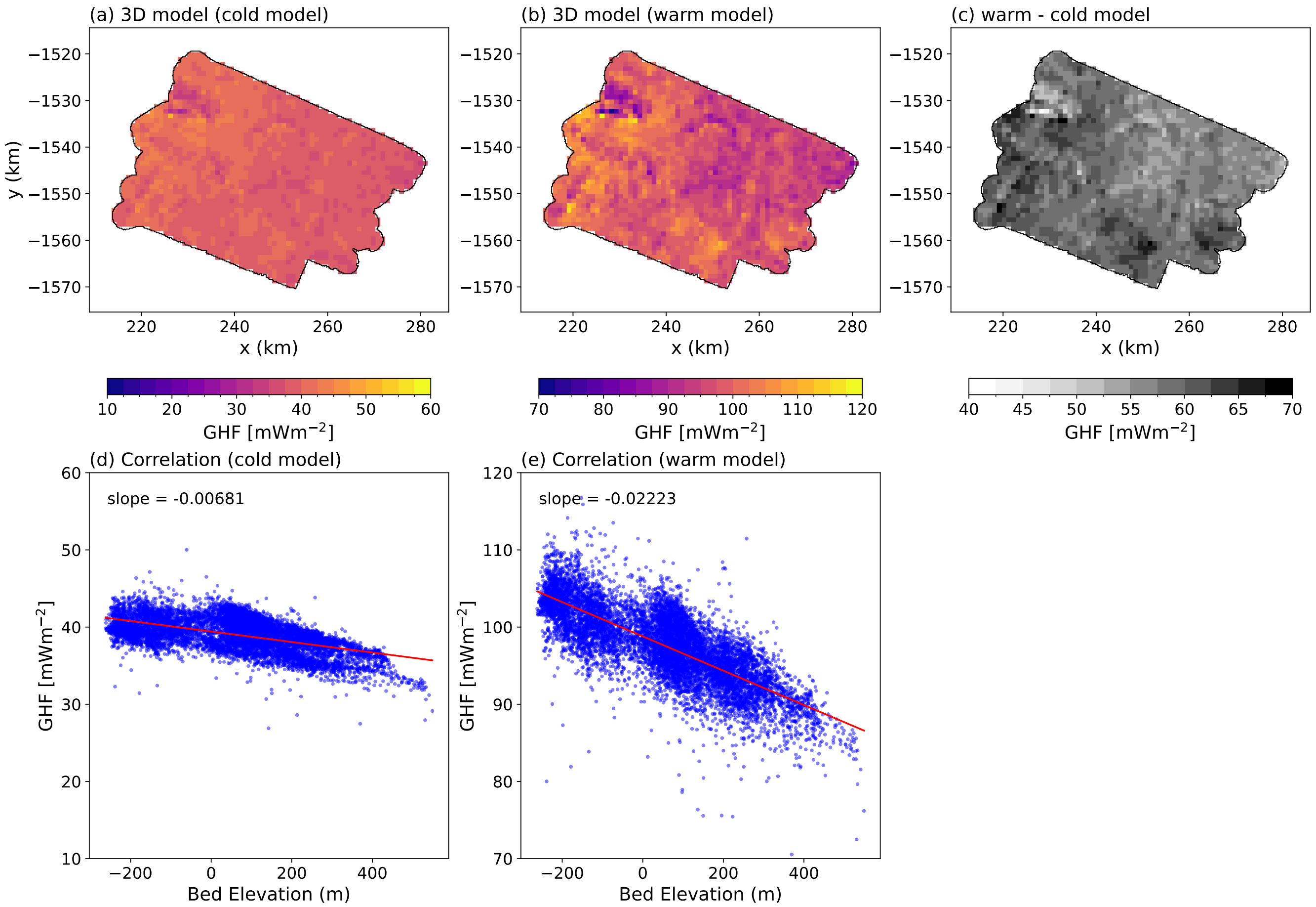

Figure 5. GHF from the 3D model using different background models. (a) the cold 3D GHF model. (b) the warm 3D GHF model. Note that different color scales are used for the 3D models due to the highly different background GHF. (c) Difference between both realizations (warm- cold model). (d) and (d) each show the correlation between the GHF and the bed elevation with the linear regression line (red) for the cold and warm 3D models, respectively.

Basal Melt Rates

The relationship between geothermal heat flow and basal melt rate is derived from a simple energy balance, assuming that the entire GHF input is used to melt ice at the base. Following Karlsson et al. (2021), the basal melt rate can therefore be calculated as

$$m_b[ma^{-1}] = \frac{q_0}{\rho_i L_f} t \qquad (2)$$

where m_b is the basal melt rate, q_0 is the GHF, ρ_i = 918 kgm^{-3} is the density of ice, $L_f = 334 \cdot 10^3$ Jkg^{-1} is the latent heat of ice, and t represents time (Karlsson et al., 2021) (Fig. 7). Because the formulation is directly proportional to q_0, the relation

https://doi.org/10.5194/egusphere-2026-4746
Preprint. Discussion started: 28 August 2026

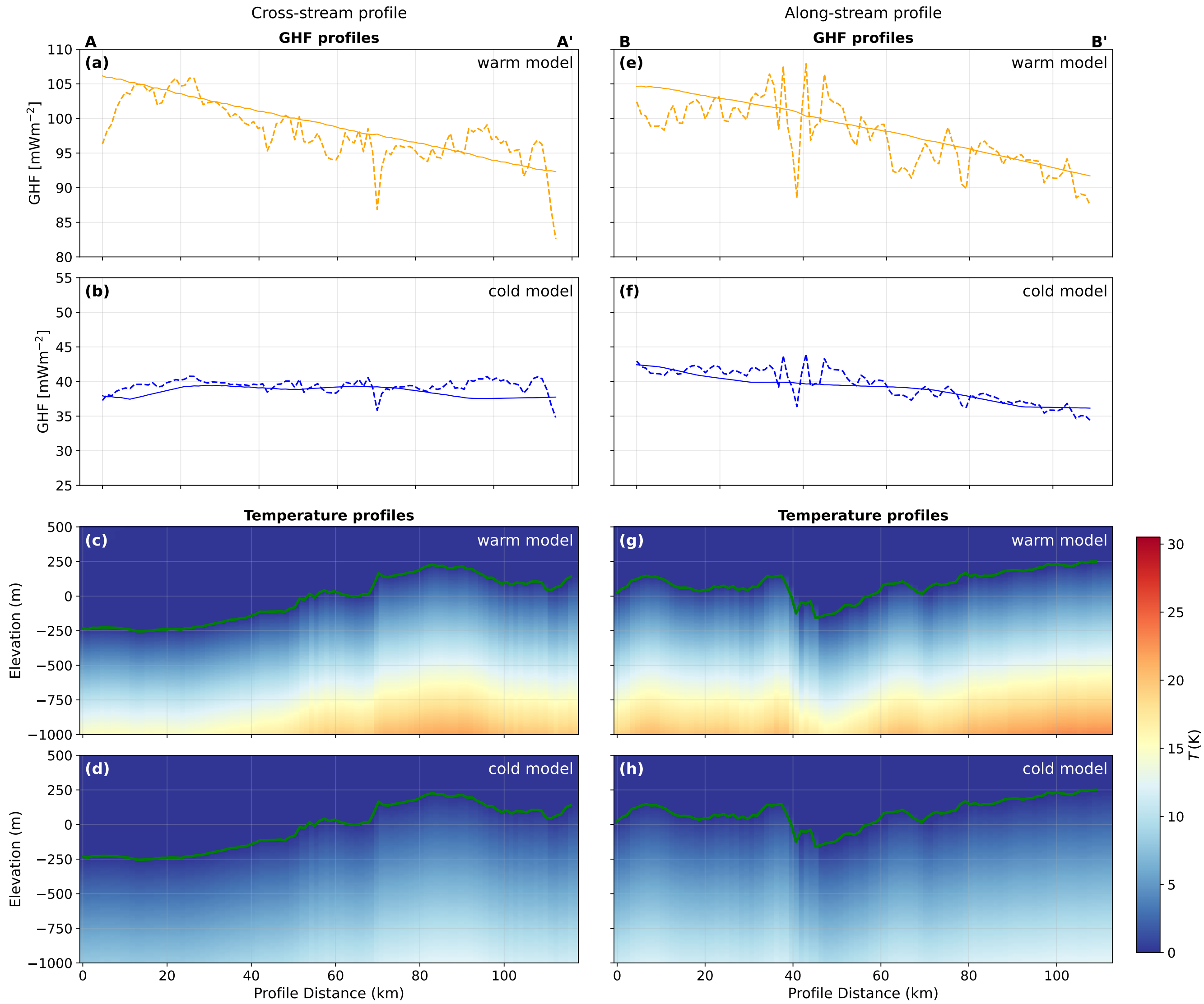

Figure 6. 2D profiles for across the ice stream (Fig. 1C, profile A-A') (a)-(d) and along the stream (Fig. 1C, profile B-B') (e)-(h). (a) and (e) show the warm 1D (orange, thin dashed) and 3D (orange, thick dashed) GHF models, (b) and (f) the cold 1D (blue, solid) and 3D (blue, dashed) GHF models. The corresponding temperature profiles for the warm model are shown in (c) and (g) and for the cold model in (d) and (h) each with the bed elevation (green) displayed.

between GHF and the basal melt rate is linear, so higher GHF produces proportionally higher basal melt rates. Comparing the 1D and 3D GHF models, the mean basal melt rates remain largely unchanged (cold models: 0.00397 $\mathrm{ma^{-1}}$ (1D) and 0.00402 $\mathrm{ma^{-1}}$ (3D), warm models: 0.01019 $\mathrm{ma^{-1}}$ (1D) and 0.01004 $\mathrm{ma^{-1}}$ (3D)). A substantial increase in basal melt rates is observed when the warm background model is used (approx. 150 % increase). Small scale variations lead to approximately

https://doi.org/10.5194/egusphere-2026-4746
Preprint. Discussion started: 28 August 2026

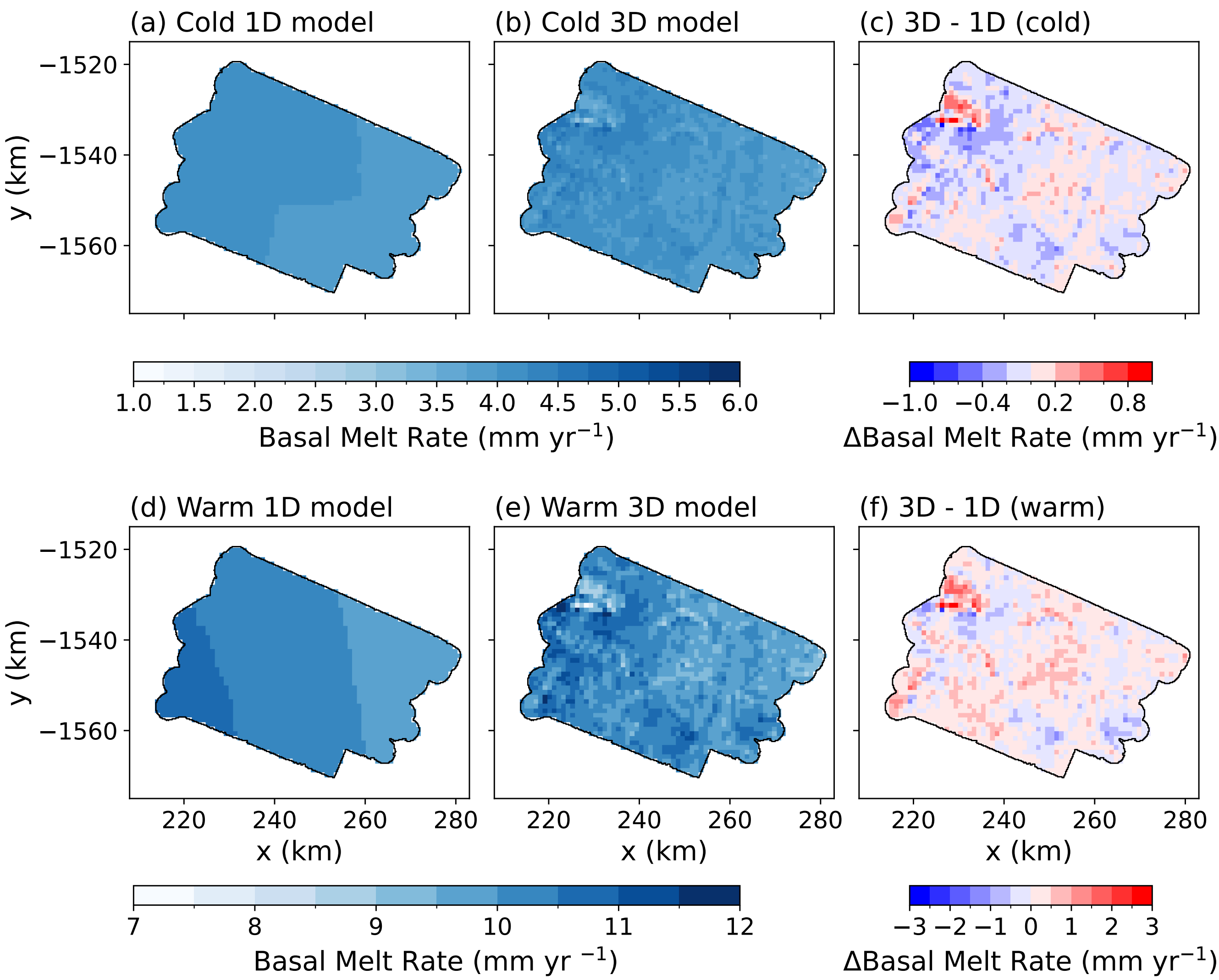

Figure 7. Basal melt calculations for (a) the 1D and (b) the 3D cold GHF models with bed elevation. (c) shows the differences between 3D and 1D. (d) - (f) show the corresponding results for the warm GHF models.

20 % variability in local basal melt rates, closely following the spatial pattern of the 3D GHF models. Within the study area, we do not identify a distinct pattern along the ice stream with strongly elevated basal melt that would contribute significantly to the dynamics of the NEGIS.

https://doi.org/10.5194/egusphere-2026-4746
Preprint. Discussion started: 28 August 2026

4 Discussion

This study demonstrates that 3D GHF modeling explicitly accounts for physically driven spatial variability in GHF, providing a more realistic representation than conventional 1D approaches. The choice of the background model primarily controls the regional mean GHF level, whereas the 3D formulation consistently introduces additional small-scale spatial variability, here linked to subglacial topography.

We identify a systematic anti-correlation between bed topography and GHF, with local 3D effects contributing up to 20% of the total variability of GHF as already observed in Colgan et al. (2021), consistent with observations in Bullard (1938); Jeffreys (1938). The 3D GHF modeling introduces additional spatial heterogeneity, especially in regions with complex bed elevation, indicating a significant contribution to the variability of GHF with high spatial resolution, as already stated by van der Veen et al. (2007). This confirms that topographic effects are not merely secondary perturbations, but represent substantial control on high-resolution GHF estimates. In contrast, the 1D steady state heat equation is widely used to estimate GHF (e.g. Lösing et al., 2020; Maule et al., 2005) in continent wide applications. In our study, it fails to capture local variations associated with high-resolution bed topography. Consequently, 1D approaches systematically underestimate the influence of complex subglacial topography.

A comparison of our GHF models with the empirical topographic correction of Colgan et al. (2021), indicates that the latter is only sensitive to horizontal variations below the radius of the imposed spatial scale parameter, here 5 km. This shows that

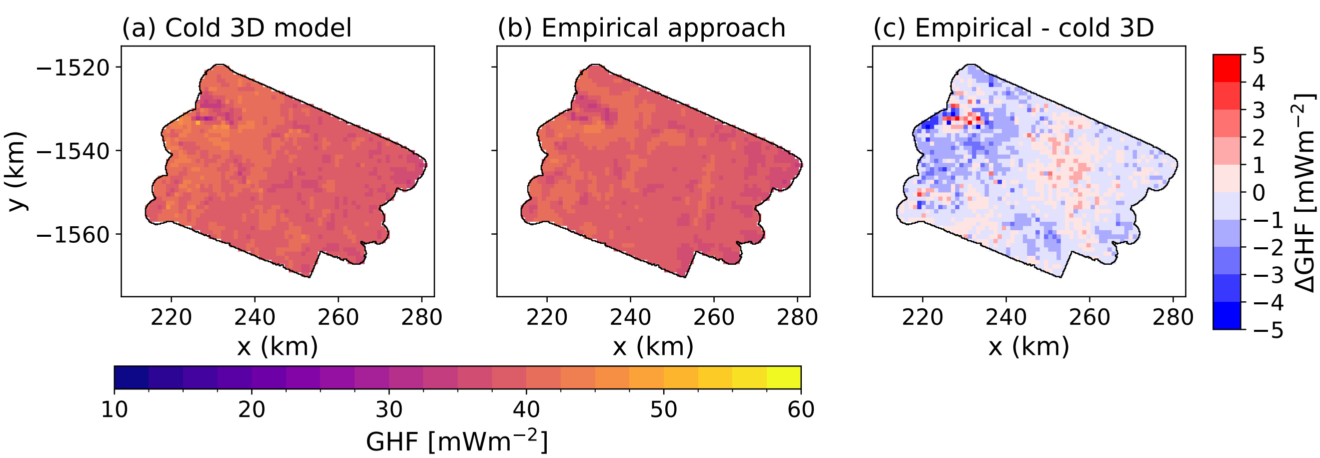

Figure 8. Comparison of (a) the cold 3D GHF model and (b) the GHF calculated with the empirical approach calculated with the cold background model and including bed topography. The difference between the models is shown in (c).

the empirical approach gives an approximation for the small-scale variability but lacks details and tends to be colder than the 3D model. Our 3D models show an additional effect of the large-scale trend of subglacial topography, resulting in 3D GHF estimates that are approximately 5-10 % higher than the estimates from the empirical approach. Additionally, the radius-based empirical approach is more susceptible to artifacts (e.g., from flight lines) than the 3D model. Although empirical approaches

https://doi.org/10.5194/egusphere-2026-4746
Preprint. Discussion started: 28 August 2026

can reproduce localized variability, they fail to capture the amplitudes and additional larger-scale topographic trends resolved by the physically based 3D modeling, resulting in systematically lower GHF estimates.

Comparisons between two background GHF models indicate that the mean GHF field is controlled by the underlying background model, whereas the 3D formulation primarily controls the local variability. The differences between the models are not uniform, but spatially structured, with the largest deviations occurring in regions of steep subglacial topography.

The observed differences in our GHF models directly translate into variations of the estimated basal melt rates. Although the choice of the background model exerts dominant control on the mean basal melt rates, the choice of model (1D/3D) significantly influences the spatial distribution of the basal melt rate. McCormack et al. (2022) show how spatially-variable GHF increases the subglacial melt rates compared to a constant model and increasing the resolution to 20 km and below might improve for example the predictions in basal melt rates. Our results indicate that both increasing the resolution of the bed topography and the model resolution (Appendix B and C) increase the variability and amplitude of GHF. The 3D simulations demonstrate that GHF contributes substantial localized variability to the basal energy budget, however, high-resolution topographic effects alone are insufficient to explain the exceptionally high basal melt rates observed beneath the NEGIS. Recent studies report basal melt rates of 0.1-0.19 $\mathrm{m\,a^{-1}}$ at the EastGRIP ice core site located in the center of our study area at NEGIS (Zeising and Humbert, 2021; Fahnestock et al., 2001; MacGregor et al., 2016). Zeising and Humbert (2021) suggested that an GHF of approximately 250 $\mathrm{mW\,m^{-2}}$ would be required to sustain such a high basal melting. However, additional processes, such as the heat supplied by subglacial water flow, likely also contribute to basal melting and were not considered in their conversion from GHF to basal melt rates (Zeising and Humbert, 2021). In contrast, our approach estimates only the direct contribution of the GHF and neglects other heat sources, including frictional heating (Karlsson et al., 2021). Consequently, our calculated melt contribution represents only a fraction of the total observed basal melt rate, as especially in the NEGIS the contribution of friction is significantly greater (Karlsson et al., 2021) and it is likely that frictional and hydrological processes dominate basal melting.

Despite improvements from incorporating bed topography, large uncertainties remain, mainly arising from limiting the appearance of small-scale variability only to topography and from the underlying model assumptions. As GHF models rely on only few direct observations (Colgan et al., 2022), large-scale models are poorly constrained, resulting in non-unique, low resolution solutions. Especially for the NEGIS, the observation at NGRIP (Dahl-Jensen et al., 2003) is a widely debated observation with an unusually high inferred GHF value (e.g. Freienstein et al., 2024; Colgan et al., 2022). Incorporating this observation into large scale models has a disproportionate influence on background GHF at the NEGIS and a potential contribution of GHF to the initiation of the ice stream (Smith-Johnsen et al., 2020a). Using the warm background GHF model from Greve (2019), which includes NGRIP, the mean GHF and the basal melt rate increase significantly by 150 %, increasing the potential of GHF to contribute to the total observed melt rate. However, the GHF model from Colgan et al. (2022), based on machine learning and integration on multiple geophysical datasets, is currently considered the most robust estimate (Lösing et al., 2025b). With this background model, the 3D topographic effect alone is insufficient to act as a primary control on the basal melt and ice stream or explain such elevated GHF as NGRIP.

Further uncertainties in small-scale variability arise from thermal and geological parameters that are not explicitly taken into

https://doi.org/10.5194/egusphere-2026-4746
Preprint. Discussion started: 28 August 2026

account in the model, but have been shown to influence small-scale variations in GHF. Bons et al. (2021) propose hydrothermal springs as a possible origin of elevated GHF at NGRIP that could strongly influence small-scale variability. Similarly, variations in radiogenic heat production have been shown to significantly influence GHF patterns on smaller-scales (Freienstein et al., 2025; Li and Aitken, 2024). Sedimentary layers can also modify GHF through thermal blanketing effects (Wangen, 1994) and are proposed to contribute to the onset of the NEGIS (Christianson et al., 2014). However, observational constraints on these processes remain sparse or generally not available at the spatial scales required to resolve the variability of GHF on the kilometer-scale. Additional constraints could improve estimates on thermal and basal properties, but, e.g., geological information is largely limited to coastal regions (Kokfelt et al., 2023), while continent-scale geological maps of Greenland (Dawes, 2009; MacGregor et al., 2024) are limited to large units and contain high uncertainties or unknown regions in central Greenland.

Despite these limitations, our study demonstrates that the 3D framework provides a flexible approach to incorporate additional spatially variable parameters into GHF estimates. In addition to the effects of the bed elevation, laterally variable radiogenic heat production reveals an additional source of small-scale variability in the 3D models. Future studies combining topographic effects with improved constraints on geology, sediments, and basal thermal parameters could further improve estimates of GHF and its influence on ice streams. Such developments have the potential to improve ice-sheet predictions and interpretations of ice stream dynamics by reducing biases introduced through simplified basal boundary conditions.

5 Conclusions

We applied a 3D thermal model to quantify the influence of high-resolution subglacial topography on GHF in the North East Greenland Ice Stream (NEGIS). To account for uncertainties in the background GHF model, we use two contrasting regional GHF models. Our results show a robust anti-correlation between the bed topography and the GHF with a local variability of up to 20 % to the background GHF. This anti-correlation is consistent across both large-scale GHF models, indicating that it is primarily controlled by the geometric effects of the bed topography. The observed large-scale GHF patterns might also be related to other 3D effects, e.g., from the variable radiogenic heat production. Compared to an existing empirical correction approach, the 3D approach allows us to include further parameters, and the results indicate a stronger correlation between the bed topography and the GHF, especially for larger-scale trends. For the NEGIS, our results suggest that small-scale variability from 3D topographic effects in GHF is unlikely to be a dominant control on the ice stream, as it does not significantly alter the overall amplitudes and variability of GHF strong enough to initialize the ice stream. The application of the approach in a different topographic setting could improve the understanding of the influence of bedrock on ice streams. Future work should focus on the variability of the thermal parameters and the inclusion of geological constraints.

Code and data availability. For our 3D modeling, we use the pyGIMli python package Rücker et al. (2017). The bed elevation data can be found in Carter et al. (2025a) for the high-resolution region at the NEGIS and in Morlighem and et al. (2022) for the BedMachine

https://doi.org/10.5194/egusphere-2026-4746
Preprint. Discussion started: 28 August 2026

v5 Greenland-wide topography. The GHF background models used are available at Colgan and Wansing (2022); Greve (2018) and the lithospheric structure was taken from Wansing (2024).

Our data are available at Freienstein (2026).

Appendix A: Relative contribution of 3D influences

We calculate the relative contribution of the 3D effects to GHF with

$$\Delta G = \frac{q_{0,3D} - q_{0,1D}}{q_{0,1D}}. \tag{A1}$$

This makes the results directly comparable to each other due to their different background models. We compare our resulting relative contributions (Fig. A1(a)-(c)) with the empirical topographic correction of Colgan et al. (2021) (Fig. A1(d)). This topographic correction calculates the 3D effect of the local elevation $z_{i,j}$ using empirically determined parameters observed in previous 3D calculations:

$$\left(\frac{\Delta q_0}{q_0}\right)_{i,j} = \frac{1}{\alpha}\left(\bar{z}_{i,j} - z_{i,j}\right). \tag{A2}$$

The characteristic height $\alpha = 950\,\mathrm{m}$ describes the local bed elevation that is necessary to change the local GHF by 100 %. The mean elevation $\bar{z}_{i,j}$ is averaged over a horizontal radius of 5 km.

We clearly see that the relative contributions are similar in magnitude and pattern for all three high resolution GHF models, however, we observe significant differences in the larger-scale trend. While the empirical topographic correction only accounts for the 3D topographic effect, the 3D calculations contain LAB and Moho depths, and RHP as additional horizontally variable parameters. To eliminate the influences of other parameters, we calculate a 3D model where LAB and Moho depth, and RHP are constant (LAB =210 km, Moho=40 km, RHP=0.5 $\mu\mathrm{W\,m^{-3}}$) and calculate the relative contribution to a 1D GHF using the same constant parameters. Thus, the relative contribution reflects the 3D effect of only the bed topography. However, we still observe a significant large-scale trend not observed in the empirical correction. The correlation plots visualize that the correlation between bed elevation and the relative contribution of the 3D calculation of the constant layer is significantly higher than the correlation between bed topography and empirical topographic correction. This could be explained by the large scale bed topography effect included in 3D and not in the topographic correction.

Appendix B: Influence of the resolution of the bed topography

We test the influence of different resolutions of the bed topography by comparing our resulting 3D GHF with the newly merged high-resolution topography with the BedMachine Topography (Fig. B1).

We observe significant differences between both results, indicating that high-resolution topography is necessary to improve the predictions of high-resolution GHF in 3D modeling.

https://doi.org/10.5194/egusphere-2026-4746
Preprint. Discussion started: 28 August 2026

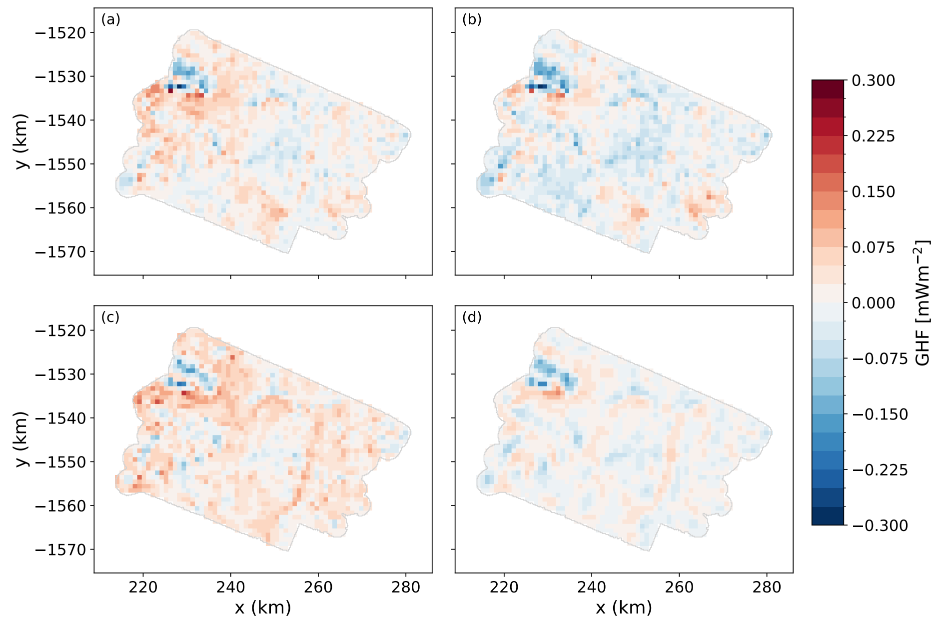

Figure A1. Relative contribution of 3D bed topography to their base GHF; (a) for the cold GHF model, (b) for the warm GHF model, (c) uses constant Moho and LAB depths and a constant radiogenic heat production, (d) is the empirically calculated topographic correction.

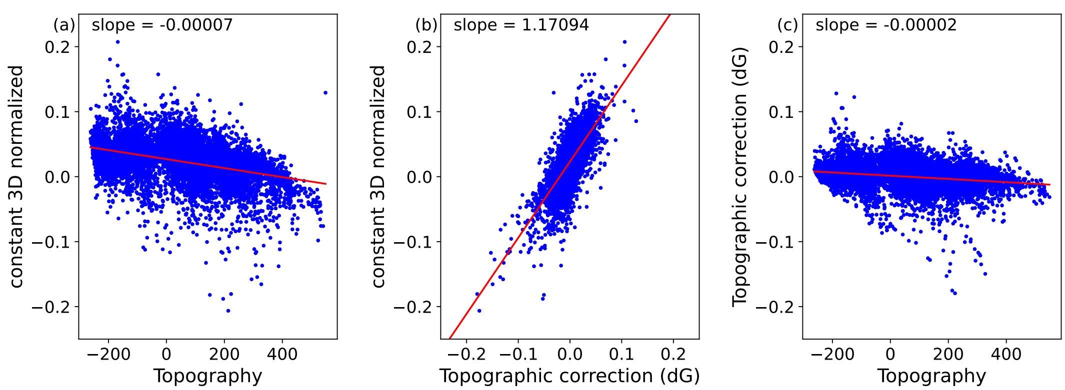

Figure A2. Comparison between the relative contribution of a constant 3D model and the empirical topographic correction. (a) shows the correlation of the constant 3D model with bed topography, (b) the correlation between the constant 3D model and the empirical topographic correction, (c) the correlation of the empirical topographic correction with bed elevation.

https://doi.org/10.5194/egusphere-2026-4746
Preprint. Discussion started: 28 August 2026

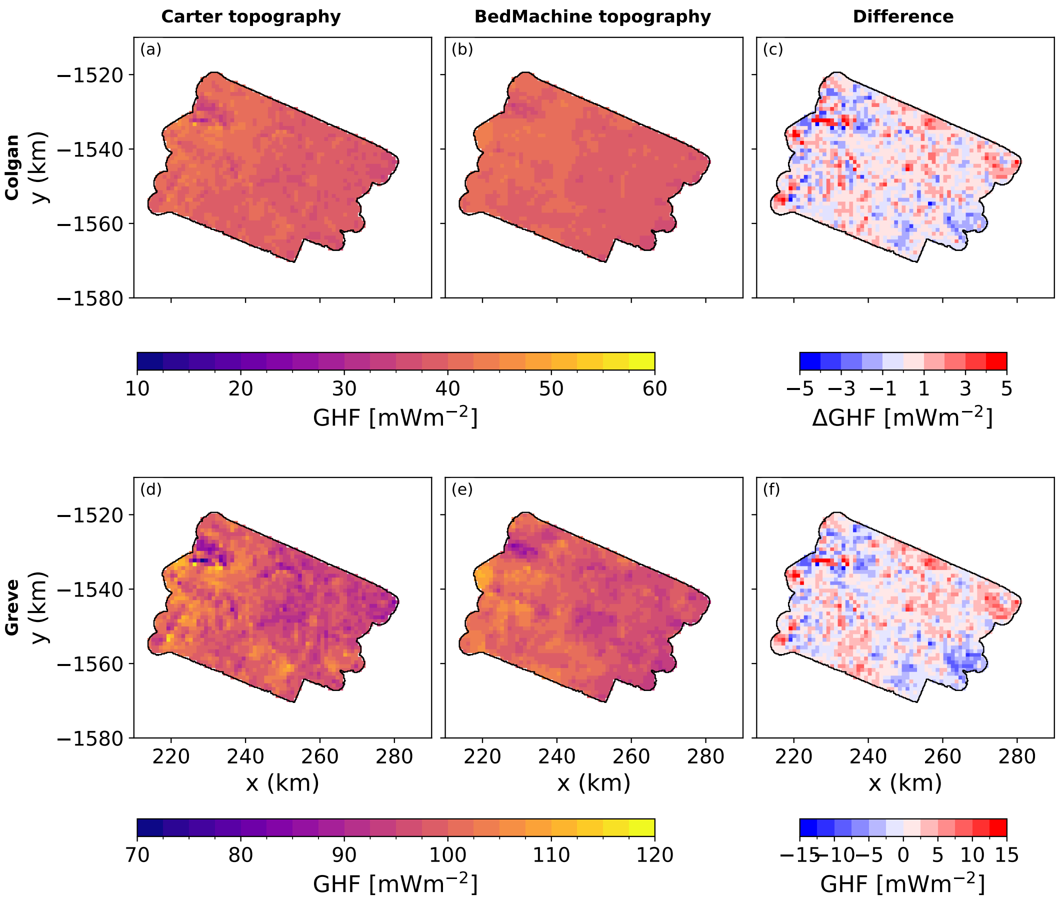

Figure B1. Comparison between the resulting 3D GHF from only the available BedMachine topography (Morlighem et al., 2017) and the merged high-resolution Carter et al. (2025a) bed topography. We show the GHF results for the cold model with (a) the BedMachine topography, (b) the merged high-resolution topography and (c) the differences from (a) and (b), as well as the results for the warm model with (d) the BedMachine topography, (e) the merged high-resolution topography and (f) the differences from (d) and (e).

Appendix C: Influence of the resolution of the 3D modeling grid

We investigate the effect of using a different resolution for the final bed topography grid. To do so, we interpolate the original 1 km resolution bed topography grid to 500 m resolution to avoid introducing effects from newly introduced topography (Fig. C1).

The results indicate that by double the final resolution of the GHF model, the GHF can vary significantly regionally with about 5 % and locally up to 25 % deviation between the two models. However, increasing the resolution also increases the computational costs significantly.

https://doi.org/10.5194/egusphere-2026-4746
Preprint. Discussion started: 28 August 2026

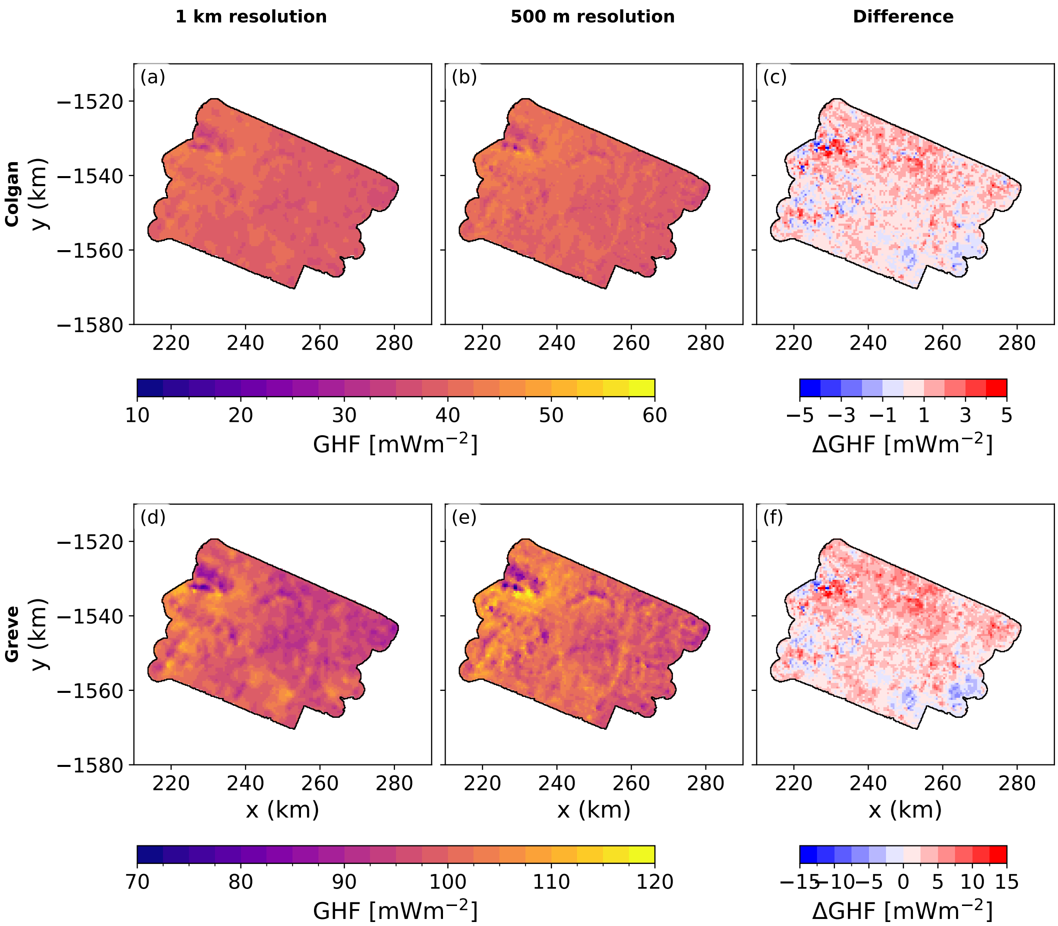

Figure C1. Comparison between the resulting 3D GHF from using a 1 km or 500 m resolution bed topography grid. We show the GHF results for the cold model with (a) the 1 km, (b) the 500 m resolution and (c) the differences from (a) and (b), as well as the results for the warm model with (d) the 1 km resolution, (e) the 500 m resolution and (f) the differences from (d) and (e).

Author contributions. JF, JE, and WS conceptualized the study and developed the methodology. JF performed the formal analysis, validated the results, prepared the visualizations, and wrote the original draft. GH and JF developed the software. CC contributed to the interpretation of the results and provided expertise on previously published datasets used in this study. OE contributed to the study design and integration of the different methodological components. JE supervised the project and administered the research. All authors reviewed, edited, and approved the final manuscript.

Competing interests. The authors declare that they have no competing interests.

https://doi.org/10.5194/egusphere-2026-4746
Preprint. Discussion started: 28 August 2026

Acknowledgements. Judith Freienstein was supported by the Deutsche Forschungsgemeinschaft (DFG) in the framework of the project "Reconciling Solid Earth and Ice Sheet Temperature Estimates for Greenland" by the following grant 535728086. Charlotte Carter was funded by the Alfred Wegener Institute's INSPIRES III programme.

https://doi.org/10.5194/egusphere-2026-4746
Preprint. Discussion started: 28 August 2026

References

Ajourlou, P., Milne, G. A., Love, R., Afonso, J. C., Salajegheh, F., Latychev, K., Kjeldsen, K. K., Lepipas, A., Martos, Y. M., and Woodroffe, S. A.: Upper mantle temperatures illuminate the Iceland hotspot track and understanding of ice–Earth interactions in Greenland, Proceedings of the National Academy of Sciences, 122, https://doi.org/10.1073/pnas.2504752122, 2025.

Aschwanden, A., Fahnestock, M. A., and Truffer, M.: Complex Greenland outlet glacier flow captured, Nature communications, 7, 10 524, https://doi.org/10.1038/ncomms10524, 2016.

Bons, P. D., de Riese, T., Franke, S., Llorens, M.-G., Sachau, T., Stoll, N., Weikusat, I., Westhoff, J., and Zhang, Y.: Comment on "Exceptionally high heat flux needed to sustain the Northeast Greenland Ice Stream" by Smith-Johnsen et al.(2020), The Cryosphere, 15, 2251–2254, https://doi.org/10.5194/tc-15-2251-2021, 2021.

Bullard, E.: The disturbance of the temperature gradient in the earth's crust by inequalities of height, Geophysical Supplements to the Monthly Notices of the Royal Astronomical Society, 4, 360–362, 1938.

Carter, C. M., Franke, S., Helm, V., Jansen, D., Paden, J. D., and Eisen, O.: High-resolution Digital Elevation Model of subglacial topography in the onset region of the Northeast Greenland Ice Stream, generated from swath radar imaging [data set], https://doi.org/10.1594/PANGAEA.972422, 2025a.

Carter, C. M., Franke, S., Jansen, D., Stokes, C. R., Helm, V., Paden, J., and Eisen, O.: Formation of mega-scale glacial lineations far inland beneath the onset of the Northeast Greenland Ice Stream, EGUsphere, 2025, 1–24, https://doi.org/10.5194/tc-19-5299-2025, 2025b.

Christianson, K., Peters, L. E., Alley, R. B., Anandakrishnan, S., Jacobel, R. W., Riverman, K. L., Muto, A., and Keisling, B. A.: Dilatant till facilitates ice-stream flow in northeast Greenland, Earth and Planetary Science Letters, 401, 57–69, https://doi.org/10.1016/J.EPSL.2014.05.060, 2014.

Chu, W., Schroeder, D. M., Seroussi, H., Creyts, T. T., and Bell, R. E.: Complex basal thermal transition near the onset of Petermann Glacier, Greenland, Journal of Geophysical Research: Earth Surface, 123, 985–995, https://doi.org/10.1029/2017jf004561, 2018.

Colgan, W. and Wansing, A.: Greenland Geothermal Heat Flow Database and Map [data set], https://doi.org/10.22008/FK2/F9P03L, 2022.

Colgan, W., MacGregor, J. A., Mankoff, K. D., Haagenson, R., Rajaram, H., Martos, Y. M., Morlighem, M., Fahnestock, M. A., and Kjeldsen, K. K.: Topographic correction of geothermal heat flux in Greenland and Antarctica, Journal of Geophysical Research: Earth Surface, 126, https://doi.org/10.1029/2020JF005598, 2021.

Colgan, W., Wansing, A., Mankoff, K., Lösing, M., Hopper, J., Louden, K., Ebbing, J., Christiansen, F. G., Ingeman-Nielsen, T., Liljedahl, L. C., et al.: Greenland Geothermal Heat Flow Database and Map (Version 1), Earth System Science Data, 14, 2209–2238, https://doi.org/10.5194/essd-14-2209-2022, 2022.

Dahl-Jensen, D., Gundestrup, N., Gogineni, S. P., and Miller, H.: Basal melt at NorthGRIP modeled from borehole, ice-core and radio-echo sounder observations, Annals of Glaciology, 37, 207–212, https://doi.org/10.3189/172756403781815492, 2003.

Dawes, P. R.: The bedrock geology under the Inland Ice: the next major challenge for Greenland mapping, GEUS Bulletin, 17, 57–60, https://doi.org/10.34194/geusb.v17.5014, 2009.

Fahnestock, M., Abdalati, W., Joughin, I., Brozena, J., and Gogineni, P.: High geothermal heat flow, basal melt, and the origin of rapid ice flow in central Greenland, Science, 294, 2338–2342, https://doi.org/10.1126/science.1065370, 2001.

Franke, S., Jansen, D., Beyer, S., Neckel, N., Binder, T., Paden, J., and Eisen, O.: Complex basal conditions and their influence on ice flow at the onset of the Northeast Greenland Ice Stream, Journal of Geophysical Research: Earth Surface, 126, https://doi.org/10.1029/2020JF005689, 2021.

https://doi.org/10.5194/egusphere-2026-4746
Preprint. Discussion started: 28 August 2026

Freienstein, J.: Dataset: 3D topographic effects on GHF beneath the NEGIS [data set], https://doi.org/10.5281/zenodo.21819972, 2026.

Freienstein, J., Szwillus, W., Wansing, A., and Ebbing, J.: Statistical appraisal of geothermal heat flow observations in the Arctic, Solid Earth, 15, 513–533, https://doi.org/10.5194/se-15-513-2024, 2024.

Freienstein, J., Szwillius, W., Zimmer, M., and Ebbing, J.: Learning from Finland: Variability of subglacial heat flow in Greenland explored from geological units and radiogenic heat production, JGR Solid Earth, https://doi.org/10.1029/2025JB031545, 2025.

Gardner, A., Fahnestock, M., Greene, C., Kennedy, J., Liukis, M., Lopez, L., and Scambos, T.: MEASURES ITS_LIVE Regional Glacier and Ice Sheet Surface Velocities, Version 2 [data set], https://doi.org/10.5067/JQ6337239C96, 2024.

Greve, R.: Geothermal heat flux distribution for the Greenland ice sheet, derived by combining a global representation and information from deep ice cores, 2.00 [data set], https://doi.org/10.17592/001.2018022701, 2018.

Greve, R.: Geothermal heat flux distribution for the Greenland ice sheet, derived by combining a global representation and information from deep ice cores, Polar Data Journal, 3, 22–36, https://doi.org/10.20575/000000, 2019.

Henriksen, N., Higgins, A., Kalsbeek, F., and Pulvertaft, T. C. R.: Greenland from Archaean to Quaternary. Descriptive text to the 1995 Geological map of Greenland, 1: 2 500 000, GEUS Bulletin, 18, 1–126, https://doi.org/10.34194/geusb.v18.4993, 2009.

Holschuh, N., Lilien, D., and Christianson, K.: Thermal weakening, convergent flow, and vertical heat transport in the Northeast Greenland Ice Stream shear margins, Geophysical Research Letters, 46, 8184–8193, https://doi.org/10.1029/2019GL083436, 2019.

IMBIE Team: Mass balance of the Greenland Ice Sheet from 1992 to 2018, Nature, 579, 233–239, https://doi.org/10.1038/s41586-019-1855-2, 2020.

Jeffreys, H.: The Disturbance of the Temperature Gradient in the Earth's Crust by Inequalities of Height., Geophysical Journal International, 4, 309–312, 1938.

Karlsson, N. B., Solgaard, A. M., Mankoff, K. D., Gillet-Chaulet, F., MacGregor, J. A., Box, J. E., Citterio, M., Colgan, W. T., Larsen, S. H., Kjeldsen, K. K., et al.: A first constraint on basal melt-water production of the Greenland ice sheet, Nature Communications, 12, 3461, https://doi.org/10.1038/s41467-021-23739-z, 2021.

Kokfelt, T. F., Willerslev, E., Bjerager, M., Heijboer, T., Keulen, N., Larsen, L. M., Pedersen, C. B., Pedersen, M., Svennevig, K., Sønderholm, M., Walentin, K. T., and Weng, W. L.: Seamless digital 1:500 000 scale geological map of Greenland, version 2.0, https://doi.org/10.22008/FK2/FWX5ET, 2023.

Krieger, L., Floricioiu, D., and Neckel, N.: Drainage basin delineation for outlet glaciers of Northeast Greenland based on Sentinel-1 ice velocities and TanDEM-X elevations, Remote Sensing of Environment, 237, https://doi.org/10.1016/j.rse.2019.111483, 2020.

Lachenbruch, A. H.: Crustal temperature and heat production: Implications of the linear heat-flow relation, Journal of Geophysical Research, 75, 3291–3300, https://doi.org/10.1029/JB075i017p03291, 1970.

Li, L. and Aitken, A.: Crustal heterogeneity of Antarctica signals spatially variable radiogenic heat production, Geophysical Research Letters, 51, https://doi.org/10.1029/2023GL106201, 2024.

Lösing, M., Ebbing, J., and Szwillus, W.: Geothermal heat flux in Antarctica: Assessing models and observations by Bayesian inversion, Frontiers in Earth Science, 8, 105, https://doi.org/10.3389/feart.2020.00105, 2020.

Lösing, M., Aitken, A. R., Ebbing, J., Halpin, J. A., Li, L., Moorkamp, M., Reading, A. M., and Staal, T.: Linking Tectonics and Crustal Thermal Properties in Southwestern Australia and East Antarctica Through Coupled Gravity and Magnetic Analysis, JGR Solid Earth, https://doi.org/10.1029/2024JB030770, 2025a.

Lösing, M., Colgan, W., Stål, T., Ebbing, J., Busck, A. G., Zhang, T., Seroussi, H., McCormack, F., Fahrner, D., Stearns, L., et al.: Community heat flow recommendations: Suitable basal boundary conditions for Greenland and Antarctica in ISMIP7, 2025b.

https://doi.org/10.5194/egusphere-2026-4746
Preprint. Discussion started: 28 August 2026

MacGregor, J. A., Fahnestock, M. A., Catania, G. A., Aschwanden, A., Clow, G. D., Colgan, W. T., Gogineni, S. P., Morlighem, M., Nowicki, S. M. J., Paden, J. D., Price, S. F., and Seroussi, H.: A synthesis of the basal thermal state of the Greenland Ice Sheet, Journal of Geophysical Research: Earth Surface, 121, 1328–1350, https://doi.org/10.1002/2015JF003803, 2016.

MacGregor, J. A., Colgan, W. T., Paxman, G. J., Tinto, K. J., Csathó, B., Darbyshire, F. A., Fahnestock, M. A., Kokfelt, T. F., MacKie, E. J., Morlighem, M., et al.: Geologic provinces beneath the Greenland Ice Sheet constrained by geophysical data synthesis, Geophysical Research Letters, 51, https://doi.org/10.1029/2023GL107357, 2024.

Martos, Y. M., Jordan, T. A., Catalán, M., Jordan, T. M., Bamber, J. L., and Vaughan, D. G.: Geothermal heat flux reveals the Iceland hotspot track underneath Greenland, Geophysical research letters, 45, 8214–8222, https://doi.org/10.1029/2018GL078289, 2018.

Maule, C. F., Purucker, M. E., Olsen, N., and Mosegaard, K.: Heat flux anomalies in Antarctica revealed by satellite magnetic data, Science, 309, 464–467, https://doi.org/10.1126/science.1106888, 2005.

McCormack, F. S., Roberts, J. L., Dow, C. F., Stål, T., Halpin, J. A., Reading, A. M., and Siegert, M. J.: Fine-Scale Geothermal Heat Flow in Antarctica Can Increase Simulated Subglacial Melt Estimates, Geophysical Research Letters, 49, https://doi.org/10.1029/2022GL098539, 2022.

Morlighem, M. and et al.: IceBridge BedMachine Greenland, Version 5 [data set], https://doi.org/10.5067/GMEVBWFLWA7X, 2022.

Morlighem, M., Williams, C. N., Rignot, E., An, L., Arndt, J. E., Bamber, J. L., Catania, G., Chauché, N., Dowdeswell, J. A., Dorschel, B., et al.: BedMachine v3: Complete bed topography and ocean bathymetry mapping of Greenland from multibeam echo sounding combined with mass conservation, Geophysical research letters, 44, 11–051, https://doi.org/10.1002/2017GL074954, 2017.

Otosaka, I. N., Shepherd, A., Ivins, E. R., Schlegel, N.-J., Amory, C., van den Broeke, M., Horwath, M., Joughin, I., King, M., Krinner, G., et al.: Mass balance of the Greenland and Antarctic ice sheets from 1992 to 2020, Earth System Science Data Discussions, 2022, 1–33, https://doi.org/10.5194/essd-15-1597-2023, 2022.

Reading, A. M., Stål, T., Halpin, J. A., Lösing, M., Ebbing, J., Shen, W., McCormack, F. S., Siddoway, C. S., and Hasterok, D.: Antarctic geothermal heat flow and its implications for tectonics and ice sheets, Nature Reviews Earth & Environment, 3, 814–831, https://doi.org/10.1038/s43017-022-00348-y, 2022.

Rücker, C., Günther, T., and Wagner, F. M.: pyGIMLi: An open-source library for modelling and inversion in geophysics, Computers and Geosciences, 109, 106–123, https://doi.org/10.1016/j.cageo.2017.07.011, 2017.

Rysgaard, S., Bendtsen, J., Mortensen, J., and Sejr, M. K.: High geothermal heat flux in close proximity to the Northeast Greenland Ice Stream, Scientific Reports, 8, 1344, https://doi.org/10.1038/s41598-018-19244-x, 2018.

Slagstad, T., Balling, N., Elvebakk, H., Midttømme, K., Olesen, O., Olsen, L., and Pascal, C.: Heat-flow measurements in Late Palaeoproterozoic to Permian geological provinces in south and central Norway and a new heat-flow map of Fennoscandia and the Norwegian–Greenland Sea, Tectonophysics, 473, 341–361, https://doi.org/10.1016/j.tecto.2009.03.007, 2009.

Smith-Johnsen, S., de Fleurian, B., Schlegel, N., Seroussi, H., and Nisancioglu, K.: Exceptionally high heat flux needed to sustain the Northeast Greenland Ice Stream, The Cryosphere, 14, 841–854, https://doi.org/10.5194/tc-14-841-2020, 2020a.

Smith-Johnsen, S., Schlegel, N.-J., de Fleurian, B., and Nisancioglu, K. H.: Sensitivity of the Northeast Greenland Ice Stream to geothermal heat, Journal of Geophysical Research: Earth Surface, 125, https://doi.org/10.1029/2019JF005252, 2020b.

van der Veen, C. J., Leftwich, T., von Frese, R., Csatho, B. M., and Li, J.: Subglacial topography and geothermal heat flux: Potential interactions with drainage of the Greenland ice sheet, Geophysical Research Letters, 34, https://doi.org/10.1029/2007GL030046, 2007.

Wangen, M.: The blanketing effect in sedimentary basins, Basin Research, 7, 283–298, https://doi.org/10.1111/j.1365-2117.1995.tb00118.x, 1994.

https://doi.org/10.5194/egusphere-2026-4746
Preprint. Discussion started: 28 August 2026

Wansing, A.: Data & Model for: The lithospheric structure of Greenland from a stepwise forward and inverse modelling approach [data set], https://doi.org/10.5281/zenodo.10691822, 2024.

Wansing, A., Ebbing, J., and Moorkamp, M.: The lithospheric structure of Greenland from a stepwise forward and inverse modelling approach, Geophysical Journal International, 238, 719–741, https://doi.org/10.1093/gji/ggae183, 2024.

Zeising, O. and Humbert, A.: Indication of high basal melting at the EastGRIP drill site on the Northeast Greenland Ice Stream, The Cryosphere, 15, 3119–3128, https://doi.org/doi.org/10.5194/tc-15-3119-2021, 2021.

Zhang, Y., Franke, S., Sachau, T., Jansen, D., Yang, H., Li, D., Hu, Y., Weikusat, I., and Bons, P.: How to make an ice stream [preprint], Research Square, https://doi.org/10.21203/rs.3.rs-5581877/v1, 2025.